Plasma Sci. Technol. **24** (2022) 124006 (16pp) https://doi.org/10.1088/2058-6272/ac9f8f

Modeling tungsten response under helium plasma irradiation: a review

Zhangcan YANG (杨章灿)* **and Junyi FAN (凡俊逸)**

Department of Nuclear Engineering and Technology, School of Energy and Power Engineering, Huazhong University of Science and Technology, Wuhan 430074, People's Republic of China

E-mail: yang_zhangcan@hust.edu.cn

Received 4 September 2022, revised 21 October 2022
Accepted for publication 2 November 2022
Published 30 November 2022

Abstract

Tungsten, a leading candidate for plasma-facing materials (PFM) in future fusion devices, will be exposed to high-flux low-energy helium plasma under the anticipated fusion operation conditions. In the past two decades, experiments have revealed that exposure to helium plasma strongly modifies the surface morphology and hence the sputtering, thermal and other properties of tungsten, posing a serious danger to the performance and lifetime of tungsten and the steady-state operation of plasma. In this article, we provide a review of modeling and simulation efforts on the long-term evolution of helium bubbles, surface morphology, and property changes of tungsten exposed to low-energy helium plasma. The current gap and outstanding challenges to establish a predictive modeling capability for dynamic evolution of PFM are discussed.

Keywords: plasma–surface interactions, tungsten, helium plasma, surface evolution, modeling and simulations

(Some figures may appear in colour only in the online journal)

1. Introduction

Tungsten, expected to be used as a plasma-facing material (PFM) in future fusion reactors, will be exposed to low-energy (20–100 eV), high-flux (10^{23}–10^{24} m^{-2} s^{-1}) helium plasma at the divertor in a fusion service environment [1–8]. In the past two decades, tungsten irradiated by helium has been studied intensively in experiments [6]. It has been widely recognized that helium bubbles are formed in tungsten under low-energy, high-flux helium irradiation. It is found that helium bubbles can form at locations far deeper than the implantation range of impinging helium ions. In general, the density and the size of helium bubbles are affected by many factors, including energy [9–11], flux and fluence of helium ions [12], irradiation temperature [13], pre-damaged state [14–17], alloying elements [18–20], surface orientation [21] and grain size of tungsten [22–24], synergistic irradiation conditions [25–27], etc. For a typical fluence ($\sim 10^{26}$ m^{-2}), the size of helium bubbles increases with tungsten temperature from 1–2 nm at low temperatures (<773 K) [13] to several tens or even hundreds of nanometers at temperatures higher than 2000 K [28].

The surface morphology of tungsten is strongly modified by low-energy helium plasma exposure, as shown in figure 1. Two types of structures have been observed to form on tungsten surfaces. One type is usually called 'fuzz' [29], alongside other names such as 'nano-structures' [30], 'nano-tendril' [31], 'coral' [32], 'nano-fiber' [6], etc. The formation conditions of fuzz have been thoroughly investigated since its discovery [29, 31, 33, 34]. The formation temperature window is between about 1000 K and 2000 K. The threshold energy of helium to induce fuzz formation is about 20 eV. The thickness of the fuzz can reach several micrometers and is demonstrated to be proportional to the square root of helium fluence minus an incubation fluence [35]. The other type of structure induced by low-energy helium plasma exposure is the pinhole structure formed at temperatures above 2000 K [28, 36]. Pinhole structures are far less studied compared to fuzz since they are less likely to form on fusion operation conditions due to the high formation temperature.

Exposure of tungsten to low-energy helium plasma can lead to changes in tungsten properties. The thermal conductivity of tungsten is dramatically reduced by the formation

* Author to whom any correspondence should be addressed.

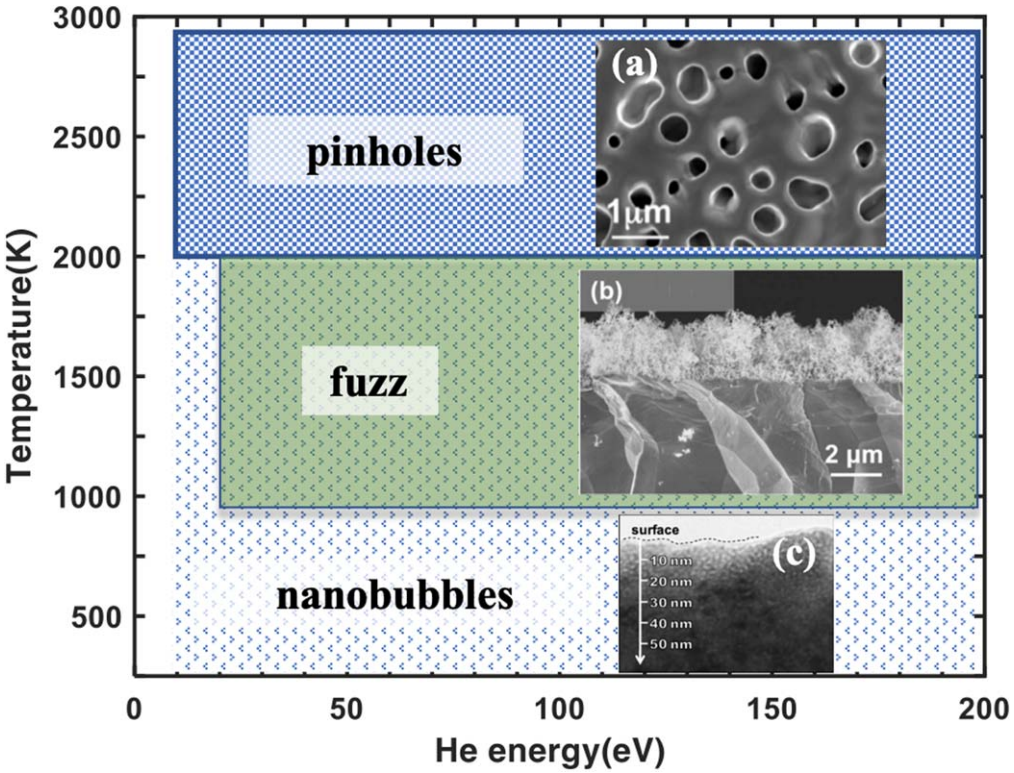

Figure 1. Modification of tungsten surfaces under irradiation with different helium energies and sample temperatures. Typical structures characterized by electron microscopy are provided as inserted images, including (a) a top view showing pinholes. Reprinted from [28], Copyright (2013), with permission from Elsevier; (b) a cross-sectional view showing fuzz. Reproduced from [37]. © IOP Publishing Ltd. All rights reserved; (c) a cross-sectional view showing a slightly rough surface and high density of subsurface nano-bubbles. Reproduced from [38], Copyright (2011), with permission from Elsevier.

of subsurface helium bubbles and surface nanostructures. It has been shown that the thermal conductivity reduces by two orders of magnitude due to the formation of subsurface helium bubbles [39]. The thermal conductivity of fuzz and pinhole structures can be as low as 1%–3% [40–42] of the bulk value. When a helium-irradiated tungsten surface is exposed to transient heat or high-flux particle loading, the significant reduction in thermal conductivity leads to enhanced erosion due to melting and splashing of the exposed surface [43–47], producing high-Z impurities in the plasma and posing a serious danger to the lifetime of tungsten and the steady-state operation of plasma. Moreover, unipolar arcing is triggered more on fuzz surfaces than on smooth surfaces, which results in more erosion [43, 48, 49]. Similar to the thermal conductivity, the physical sputtering yield of fuzz is significantly lower than that of smooth surfaces. It is found that the sputtering yield of fuzz decreases with the increase of fuzz thickness and saturates at a value about 8%–10% of that of smooth surfaces [37, 50]. Exposure to helium plasma also influences the retention of hydrogen isotopes in tungsten. Baldwin *et al* pointed out that the formation of a subsurface nano-bubble layer reduced deuterium retention by a factor of 100–1000, while deuterium retention in the fuzz layers seemed to be very low [27].

The above introduction provides a short summary of the experimental efforts to understand the tungsten response under helium plasma exposure. According to these experimental results, we can conclude that exposure to helium plasma causes damage to the lifetime of tungsten and the safe operation of fusion devices. However, there are still challenges in accurately predicting the properties and performance of tungsten in a real fusion reactor based on the existing experimental studies. Firstly, most of the reported experiments used linear plasma devices to emulate helium plasma exposure in a tokamak divertor. Compared to linear plasma devices, plasma loading conditions in fusion devices have several differences, including grazing incident angles, energy distribution, presence of recycling and re-deposition of sputtered atoms, and inclusion of impurity species [31], all of which could potentially influence the dynamics of bubble growth and surface evolution. Secondly, besides helium plasma, tungsten will also be exposed to high-energy neutrons, hydrogen plasma and heat in a fusion reactor. Due to the lack of real fusion facilities, the synergistic effects of neutron irradiation, helium/hydrogen plasma exposure and heat loading are less explored. Lastly, the detailed mechanism of helium-induced damage relies on microscopic processes which are difficult to access experimentally.

Modeling and simulations have been conducted in complement to experimental efforts to understand the mechanism of bubble formation and growth, changes in surface morphology and thermo-mechanical properties, with the ultimate goal to establish a model or a framework with predictive capability for fusion operation conditions. Numerous density functional theory (DFT) and molecular dynamics

(MD) studies have been carried out to study the thermodynamic and kinetic properties of helium atoms and clusters, helium interactions with various types of defects, the mechanism of helium bubble nucleation and growth, and the evolution of surface morphology at early stages. The information obtained from these atomic-level simulations will be passed to higher-level simulations to predict the long-term performance of tungsten.

The emphasis of this review will be on modeling and simulation efforts on the long-term evolution of helium bubbles, surface morphology, and property changes of tungsten, which are less covered in existing reviews on the topic of tungsten damaged by helium irradiation, such as references [4–6, 8, 51, 52]. The aim of this article is to overview the recent progress, gaps and challenges in the modeling of surface evolution and to evaluate the readiness of coupling subsurface bubble accumulation, surface evolution, property change and edge plasma physics. It is noted that the scope of this review is limited to low-energy helium plasma exposure of tungsten surfaces. Particular attention will be paid to the effects of surfaces on helium behavior. Helium bubble growth in the bulk or high-energy helium irradiation is not covered in this article.

This article is organized as follows. This section provides a brief overview of the experimental results of tungsten exposed to helium plasma. Section 2 summarizes the microscopic studies of helium implantation, helium bubble nucleation and growth. Section 3 describes the modeling efforts on the long-term evolution of helium bubbles and surface morphology, and the integration of a multi-physics model. Section 4 provides an overview of modeling approaches to understand the sputtering yield and thermal properties of tungsten after exposure to helium plasma. Finally, we give a summary in section 5.

2. Helium bubble nucleation and growth

2.1. Implantation of helium and depth distribution

As a helium ion moves towards a tungsten surface, it may reflect from the surface or implant into the surface. The reflection coefficient depends on the ion energy, ion incidence angle and surface orientation of tungsten. SRIM (Stopping and Range of Ions in Matter) [53] and MD are the two main simulation methods to obtain the reflection coefficient. Henriksson *et al* [54] performed MD simulations of helium atom bombardment of tungsten surfaces with helium energy ranging from 20 to 200 eV at an off-normal angle of 25°. It was found that almost all helium atoms with energy of 20 eV were reflected from the surface. The reflection coefficient decreased with increasing ion energy and reached about 0.6 for 200 eV. In comparison, the reflection coefficient predicted by SRIM was about 0.5 in the range of 20–200 eV. Pentecoste *et al* [55] studied the cumulative bombardment of 300 eV helium into tungsten surfaces using MD. They found that the reflection coefficient increased as helium accumulated at the surface. Hammond *et al* [56] systematically studied crystal orientation

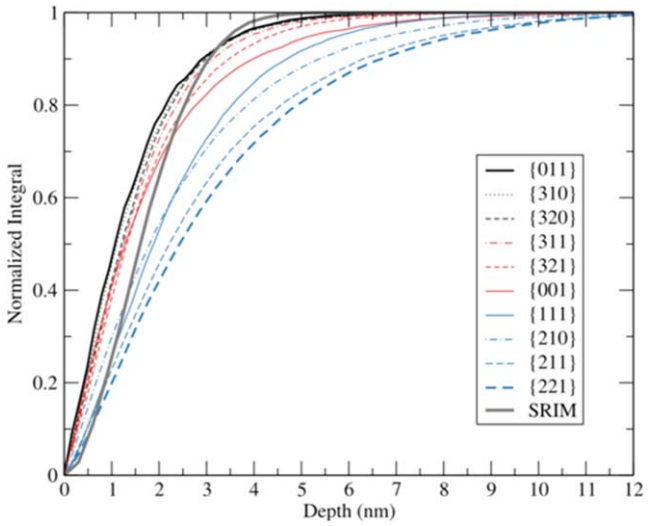

Figure 2. Cumulative depth distribution of helium atoms for different surface orientations. Reprinted from [56], with the permission of AIP Publishing.

effects on helium reflection using MD. They found that the reflection coefficient for 100 eV helium atoms varied for different surface orientations ranging from 0.46 to 0.65, while SRIM predicted a value of 0.44 and could not account for the effects of surface orientations. The above studies show a clear difference in the reflection coefficient between the MD and SRIM results for low-energy bombardments. The difference is due to the importance of many-body atomic interactions at low energies, which are included intrinsically in MD but not SRIM [54]. Thus, for low-energy bombardments, binary collision approximation (BCA)-based approaches such as SRIM cannot provide reliable results at least for the reflection coefficient. A reflection coefficient of 100% for energy lower than 20 eV predicted by MD may explain the threshold energy for pinhole and fuzz formation. Helium atoms need to overcome a surface barrier to be embedded into tungsten.

When a helium atom penetrates into tungsten, it is slowed down by collisions with tungsten atoms. Due to the low energy of the helium atom and the large difference in mass between helium and tungsten, the collisions cannot cause any displacement damages since the transferred energy to the recoil is below the threshold displacement energy [22]. After the helium atom slows down, it usually sits at the interstitial sites. The implantation depth distribution of helium at rest can be obtained by MD or SRIM simulations. Using MD simulations, Hammond *et al* [56] found that the helium depth distribution depends on the surface orientation as shown in figure 2. Surfaces with denser areal density such as {0 1 1} surfaces have the shallowest depth profile, while helium atoms go deeper for more corrugated surfaces such as {2 1 1} surfaces. SRIM results are different from MD results because SRIM does not consider the atomic arrangement. Moreover, SRIM considers electronic stopping which is not modeled in MD.

The depth profile of as-implanted helium is useful for simulations of long-term evolution. Since impinging helium ions do not cause any displacement damage, the detailed

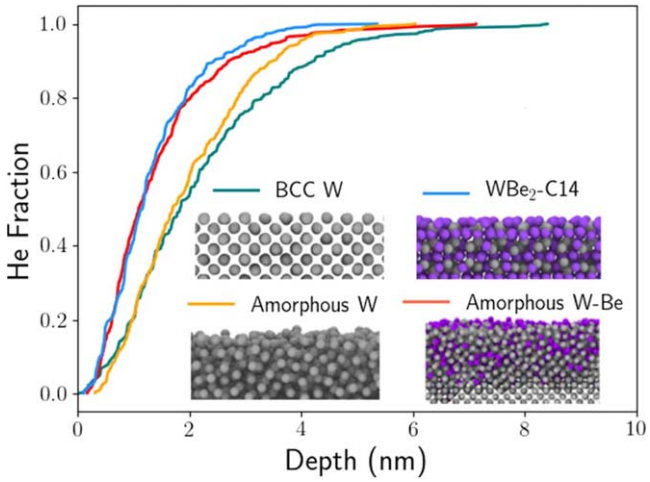

Figure 3. Cumulative depth distribution in pure tungsten and tungsten–beryllium surfaces. Reproduced from [61]. © IOP Publishing Ltd. All rights reserved.

process of slowing down can be ignored to save computational time. Thus, in several MD simulations [57], helium atoms are inserted directly into a simulation box according to the corresponding depth distribution. Depth distribution has also been used as a source term for helium in simulations aiming for long-term evolution, such as object kinetic Monte Carlo (OKMC) [58] and cluster dynamics (CD) [59] simulations. It is worth noting that most studies used implantation depth profile calculated by SRIM rather than MD, which could introduce uncertainties to the results especially for low-energy bombardments [60].

All these studies were performed on smooth surfaces of a single crystal. In fusion operation conditions, impurities such as beryllium can be deposited on the surface, changing the surface chemistry. Recently, Cusentino *et al* [61] pointed out that the deposition of beryllium shifts the helium implantation depth distribution to a shallower profile compared to a pure tungsten surface, as shown in figure 3. This means that more helium atoms are implanted closer to the surface and the escape of helium out of the surface is easier, leading to suppression of helium bubble formation. Therefore, the effects of impurity deposition on the implantation depth profile need to be taken into account when simulating realistic fusion operation conditions. Moreover, when surface structures evolve, the implantation process is also very different. We discuss the transport of helium ions in fuzz layers in section 3.2.

2.2. Helium bubble nucleation

Single helium atoms at interstitial sites are very mobile in tungsten. The diffusion barrier calculated by Becquart and Domain [62] using DFT is only 0.06 eV. MD simulations have also been used to calculate the diffusion barrier mainly based on the mean square displacement approach. The obtained values of the barrier vary for different tungsten–helium interatomic potentials, e.g. 0.11 eV and 0.13 eV by Wang *et al* [63], 0.13 eV by Faney *et al* [59], 0.15 eV by Perez *et al* [64], 0.021 eV and 0.157 eV by Shu *et al* [65]. Due to such a low diffusion barrier, single helium atoms diffuse very fast in tungsten even at low temperatures.

Nucleation of helium bubbles is achieved in two main ways [58]. The first one is by the self-trapping mechanism without the aid of any other defects. DFT calculations have revealed that helium interstitial atoms are attracted by each other. The total binding energies of He_2, He_3, He_4 and He_5 clusters are 1.03 eV, 2.39 eV, 3.90 eV and 5.54 eV, respectively [62]. As a result, an interstitial cluster of helium atoms grows by absorbing mobile helium atoms. As the size of a helium cluster becomes larger, the local stress exerted by the helium cluster causes larger lattice distortion, as illustrated in figures 4(a)–(f). When the size of the helium cluster reaches a critical value, the helium cluster is able to completely push out a lattice tungsten atom, creating a Frenkel pair. The helium cluster then moves to the created vacancy site to form a helium–vacancy (He–V) complex, as shown in figure 4(g). This process is called 'trap mutation.' Using MD, Perez *et al* [64] found that the mutation rate increases sharply with helium cluster size and temperature, as shown in figure 5. The energy barrier of the trap mutation process decreases from 1.20 eV for He_5 to 0.7 eV for He_7. Boisse *et al* [66] also studied the trap mutation process using both MD and DFT. They found that it is energetically more favored for a pure helium cluster with a size larger than 6 to undergo trap mutation. The mobility of He–V complexes is usually ignored, especially for low temperature. Consequently, such He–V complexes can act as nucleation sites for helium bubbles.

The other mechanism of helium bubble nucleation is by helium trapping to existing defects. Helium atoms are found to be attracted to almost all types of defects, including vacancies, interstitials, impurity atoms (e.g. C), dislocations, grain boundaries, etc [68–72]. In particular, a helium atom binds very strongly with a vacancy with a binding energy of 4.57 eV as calculated by DFT [68]. Such a He–V complex can absorb more mobile helium atoms or vacancies [71] to form nano-bubbles.

It is difficult for bubble nucleation via the self-trapping mechanism to occur for low incident fluxes ($<10^{20}$ m^{-2} s^{-1}). However, the self-trapping mechanism becomes dominant at high fluxes. For instance, the formation of a high density of helium bubbles has been observed by many MD simulations with helium fluxes larger than 10^{25} m^{-2} s^{-1} [55, 73, 74]. Since there are no pre-existing traps in these MD simulations, the formation of bubbles can only be attributed to the self-trapping mechanism. Using OKMC simulations, Yang *et al* [58] found that the helium bubble formation mechanism is strongly dependent on the temperature and concentration of pre-existing traps for ITER relevant conditions with helium fluxes in the range of 10^{22}–10^{24} m^{-2} s^{-1}. For 50 appm (atom parts per million) of pre-existing traps, the self-trapping mechanism may be dominant in the low-temperature regime (<400 K). However, this finding is difficult to be verified by experiments reported in literature. In practice, most commercial tungsten materials used in experiments have a purity of 99.99%, which means that the impurity concentration is at least 100 appm. These impurities can act as potential traps for helium bubble nucleation. As a

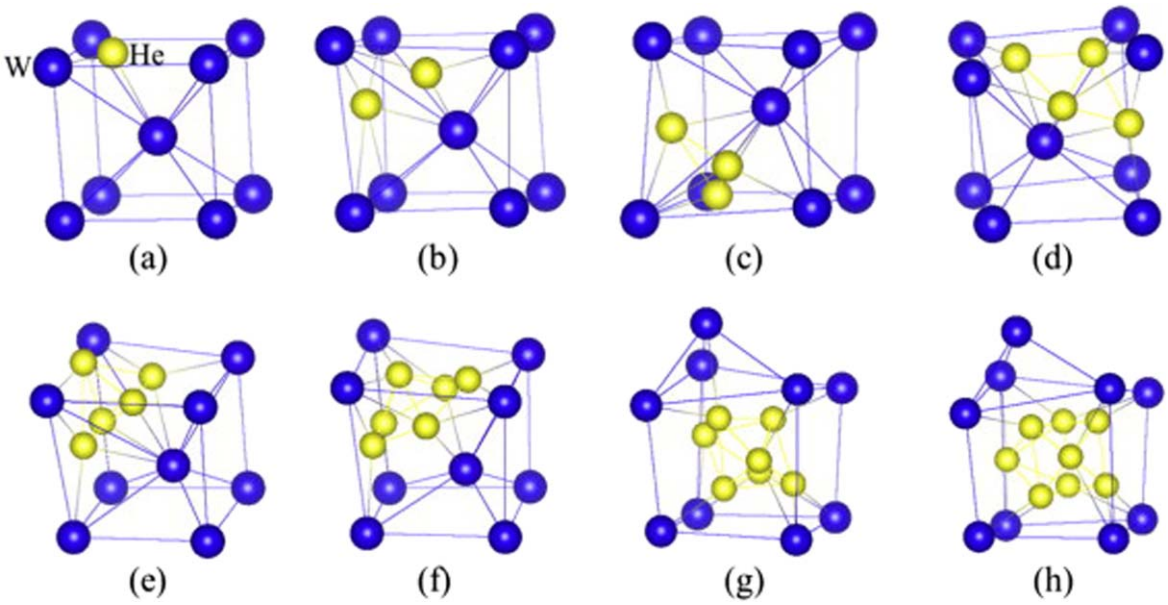

Figure 4. Configuration of He_n clusters predicted by MD simulations. Blue and yellow spheres represent tungsten and helium atoms, respectively. Reprinted from [67], Copyright (2014), with permission from Elsevier.

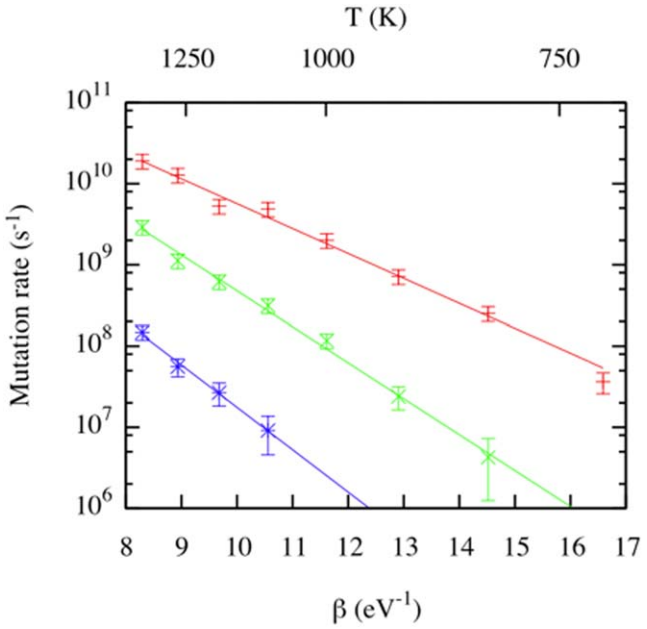

Figure 5. Mutation rate as a function of inverse temperature β. Red, green, and blue symbols represent He_7, He_6, and He_5, respectively. The lines are Arrhenius fits. Reprinted (figure) with permission from [64], Copyright (2014) by the American Physical Society.

result, it is hard to distinguish whether the bubbles are formed due to the self-trapping or impurity-trapping mechanism without detailed characterizations.

Since helium atoms are implanted only a few nanometers beneath the surface, it is important to take into account the effect of surfaces on helium bubble nucleation. MD simulations have revealed that nucleation is enhanced due to the elastic interaction between helium clusters and the surfaces. Hammond *et al* [56] indicated that one helium atom is sufficient to cause trap mutation under {1 1 1} surfaces. Lin *et al* [75–77] carried out systematic simulations of small mobile helium clusters near tungsten surfaces. They found that helium clusters located about 10–20 atomic layers below the surface can feel the elastic interaction of the surfaces. As helium clusters move to the surface, trap mutation is activated at rates much higher than in the bulk. The increase in helium nucleation near the surface needs to be taken into account since this leads to a drift transport of helium toward the surface and helium segregation on the surfaces [78]. The rate of nucleation is also higher near helium bubbles [79] and grain boundaries [76, 80], leading to the formation of a helium bubble network [81] and accumulation of helium at grain boundaries [76].

2.3. Helium bubble growth

Helium bubbles can grow by absorbing vacancies and helium atoms. In situations where vacancies are absent (e.g. irradiation of pure tungsten with low-energy helium plasma) or immobile (e.g. low temperature), helium bubbles become over-pressurized due to the high helium to vacancy ratio. When the pressure of the bubble reaches a critical value, it pushes out tungsten atoms to release its pressure. The generated self-interstitial atoms (SIAs) stay around the bubble at first, and then organize and form a prismatic dislocation which is finally detached from the bubble. This process is called 'loop punching' [73, 82]. The size of the bubble increases due to the creation of vacancies during this process.

The coalescence of helium bubbles is another way for the formation of large helium bubbles and becomes important for the situations where a high density of bubbles is formed. The coalescence phenomenon has been observed in both experiments [13, 36] and MD simulations [55, 73, 74]. Smirnov *et al* [83] used MD to study the continuous growth of two adjacent helium bubbles until coalescence, and found that the

Table 1. List of reactions related to He_nV_m clusters. Reproduced from [86].

Reaction		Formula	Comment
Clustering reactions	Helium clustering	$He_x + He_y \rightarrow He_{x+y}$	Only possible for small clusters due to trap mutation for large $x + y$
	He/V clustering	$He_x + V_y \rightarrow He_xV_y$	
	He/V cluster growth through helium absorption	$He_xV_y + He_z \rightarrow He_{x+z}V_y$	
	He/V cluster growth through single vacancy absorption	$He_x\ V_y + V \rightarrow He_x\ V_{y+1}$	
	He/V cluster reduction through interstitial absorption	$He_x\ V_y + I_z \rightarrow He_x\ V_{y-z}$	
Dissociation reactions	Helium dissociation	$He_xV_y \rightarrow He_{x-1}V_y + He$	Single He dissociates from cluster
	Vacancy dissociation	$He_x\ V_y \rightarrow He_x\ V_{y-1} + V$	Single vacancy dissociates from cluster
	Trap mutation	$He_x\ V_y \rightarrow He_x\ V_{y+1} + I$	High-pressure He/V cluster ejects a lattice atom to create a single interstitial

two growing helium bubbles repel each other during the coalescence process. Zhan *et al* [84] simulated the coalescence conditions of small-sized helium bubbles (with a radius of 1–3 lattice constants). They found that the helium bubbles can coalesce when the distance between the two helium bubbles is less than one lattice constant. Xu *et al* [85] performed systematic MD simulations to investigate the factors affecting bubble coalescence, including the relative positions of the helium bubbles, the temperature, the helium to vacancy ratio, and the distance between helium bubbles. They found that helium bubbles arranged along the ⟨100⟩ direction is easier to coalesce than those arranged along the ⟨111⟩ direction. High temperature and high helium to vacancy ratio can promote coalescence.

3. Long-term evolution of helium accumulation and surface morphology

3.1. Long-term evolution of helium bubbles

OKMC and CD are the two main coarse-grained simulation methods to study the long-term evolution of helium bubbles. Both approaches are widely used to study microstructure evolutions of materials under irradiation. These two approaches rely on the physical processes and corresponding parameters usually determined from DFT or MD simulations.

In long-term simulations, the evolution of the pressure in helium bubbles is not modeled in a direct way. Instead, the evolution of helium bubbles is controlled by the binding energies and helium to vacancy ratio. Based on the knowledge gained from DFT and MD simulations, a list of possible reactions related to He_nV_m clusters is compiled in table 1. Due to the positive binding energy of He or V to He_nV_m clusters, clustering reactions are usually assumed to occur spontaneously as long as the He or V is within the capture distance of He_nV_m clusters. The dissociation reactions are governed by the dissociation activation energy, which is a sum of the binding energy and the diffusion energy barrier of the emitted species. The clustering and dissociation reactions lead to the change of n and m in He_nV_m, indicating the growth or shrinkage of He_nV_m. The helium to vacancy ratio n/m is an indicator of the bubble pressure. Since trap mutation can happen for high-pressure bubbles, the value of n/m in He_nV_m is limited to a certain range. For instance, in the long-term simulations by Faney *et al* [86] and Yang *et al* [58], n/m is limited to be smaller than 4 according to MD simulations. Once n/m is larger than 4, the trap mutation reaction is assumed to occur.

The OKMC approach tracks all defects in a simulation box, ignoring lattice tungsten atoms. Defects are treated as objects. All possible events (diffusion, emission, annihilation, agglomeration, etc) of these objects are identified to construct an event list. An event is randomly picked to be carried out based on its weighted rate. The system advances by repeating the previous steps. A more detailed principle of this approach can be found in [87]. By parameterization with *ab initio* calculations, Becquart *et al* [68, 88] successfully reproduced a helium desorption experiment using OKMC. Yang *et al* [58] explored the effects of pre-existing vacancies on near-surface helium accumulation under a broad range of irradiation conditions. They evaluated the relative contribution of helium nucleation due to helium self-trapping or vacancy trapping by evaluating the proportion of retained helium due to self-trapping. Figure 6 is a compilation of the results. As clearly seen in figure 6, the self-trapping mechanism is completely dominant for high-flux implantation conditions. The importance of the vacancy-trapping mechanism increases as temperature increases. Nandipati *et al* [89] investigated the effect of helium flux on helium bubble behavior in more detail. They found that nearly no helium was retained near the surface for low fluxes (10^{22} m^{-2} s^{-1}) without pre-existing traps, which is in good agreement with the results by Yang *et al* [58]. They pointed out that low fluxes increase the diffusion time of mobile helium and hence increase the escape probability of helium to the free surface. As a result, helium retention decreases as flux decreases. Their results also agree well with MD results [74] at low fluence. Overestimation of helium retention at higher fluence is due to no implementation

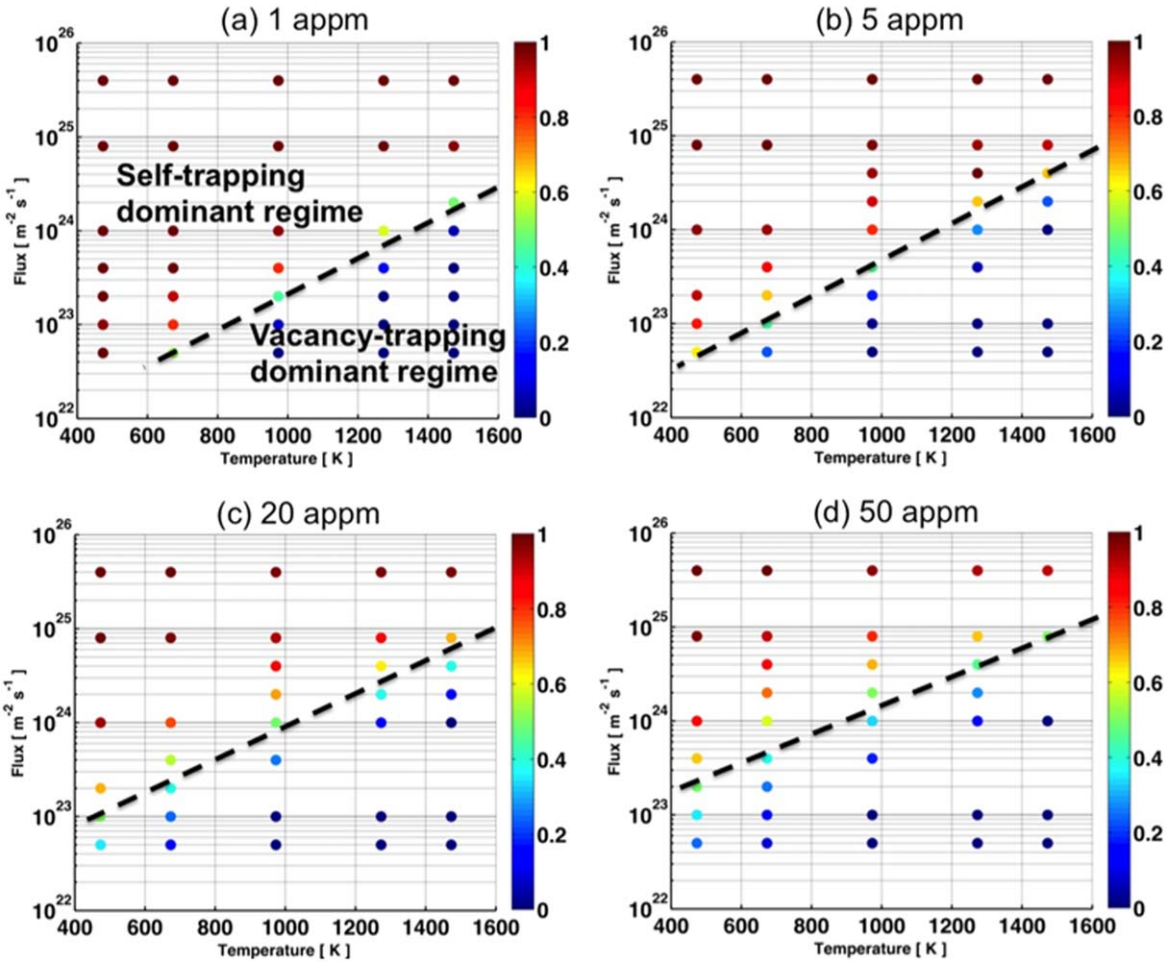

Figure 6. Phase diagram of the relative contribution of helium self-trapping to helium retention. A value of '1' means that self-trapping completely dominates. A value of '0' means that self-trapping can be ignored. The dashed lines denote where the contribution of self-trapping equals that of vacancy trapping. [58] [2017], reprinted by permission of the publisher (Taylor & Francis Ltd, http://www.tandfonline.com).

of bubble rupture in their OKMC model. There are several other OKMC simulations reported in the literature that investigate the effects of certain physical processes on bubble evolution. For instance, Ma *et al* [90] and Hou *et al* [91] studied the collaborative motion of helium and SIAs and found that a helium atom changes the motion pattern of an SIA from one-dimensional (1D) migration to three-dimensional (3D) migration. As a result, the annihilation rates between vacancies and SIAs are increased.

Although OKMC is capable of achieving temporal and spatial scales several orders of magnitude larger than MD simulations, the reported OKMC studies [58, 74] were mainly for validation of parameterization and to provide insights for MD results. For future studies, OKMC can play a more important role in understanding long-term evolution of bubbles if the simulation time is extended and more physical processes are implemented in the model. OKMC studies can also serve as a bridge to provide crucial parameters (e.g. sink strength [92]) for larger-scale simulations, such as CD.

The timescale that can be achieved by CD is much longer. CD provides the capability to simulate bubble evolution for the lifetime of tungsten in a fusion device. The fundamental principle of the CD approach is the mean field rate theory, which assumes that defects are uniformly distributed in materials and that the reaction between defects is like chemical reactions of reactants in a solution. Thus, by solving a set of diffusion-reaction rate equations, CD tracks the concentration of defects, ignoring the spatial information of individual defects. The success of CD simulations mainly relies on whether the model captures the most important physical processes and the accuracy of the parameters related to these processes [93, 94].

Significant progress has been made in CD simulations of helium accumulation in tungsten. Watanabe *et al* [95] studied the mechanism of interstitial loop formation in tungsten irradiated with 8 keV helium ions at 300 K. They found that the dynamic trapping and de-trapping of the interstitial atoms from He–V complexes is a key process for interstitial loop nucleation. Qu *et al* [96] compared helium retention in two cases relevant to tungsten irradiation at the first wall and the divertor target. They found that the case with high-flux ($10^{22}\,\mathrm{m^{-2}\ s^{-1}}$), low-energy (30 eV) helium plasma leads to more helium retention than the other case irradiated by low-flux ($10^{18}\,\mathrm{m^{-2}\ s^{-1}}$), high-energy (1 keV) helium ions at

873 K. In order to overcome the limitation that only single-vacancy, single-interstitial and small-He_nV ($n = 1$–6) complexes were considered in the CD model of Qu *et al* [96], Li and coworkers [97] developed a CD model that can take into account vacancy clusters, interstitial clusters and He_nV_m complexes. They used this new CD model to simulate keV-ion beam irradiation experiments, fusion-relevant irradiation conditions [98] and effects of grain size on helium retention [99]. Reasonable agreement was achieved with experimental results in terms of the depth profile of helium concentration.

The CD model by Li and coworkers [97] is suitable for irradiation conditions where incident ions can induce displacement damages and are implanted deep in tungsten, whereas the model is not so effective at addressing helium accumulation for low-energy helium plasma exposure where no displacement damages are produced and the implantation depth of helium is only a few nanometers below the surface. Moreover, helium accumulation near surfaces is responsible for the evolution of surface morphology. As a result, when dealing with low-energy, high-flux helium plasma exposure and the induced surface structures, surfaces cannot be simply treated as a defect sink. The elastic interaction between mobile helium clusters and the surface has to be considered.

In light of the importance of surface effects, the Wirth group from the University of Tennessee and their collaborators have developed a spatially dependent drift-diffusion-reaction CD code in the past decade. The first version of the code was reported in 2014 [59]. Built upon MD simulations, the behavior of helium clusters was modeled more accurately in this CD model. Diffusion of small helium clusters, trap mutation, and dissociation of He_nV_m complexes were taken into account. The associated energy barrier and rate coefficients were determined from either atomistic simulations or experiments. This code was used to study the effects of helium flux and temperature on helium accumulation and strong correlation was found [86]. Krasheninnikov *et al* [100, 101] used a reduced version of the CD model to study helium accumulation in fuzz tendrils and slab surfaces. One interesting finding was that helium clusters cannot form in a tendril without pre-existing defects. This reduced model was also used to study the effects of helium bubble induced formation of traps on helium accumulation [102]. In 2015, the code was significantly improved by integration of the drift process and the modified trap mutation process [78] and the code was named 'Xolotl'. Figure 7 shows cumulative helium distributions with and without considering processes of drift and modified trap mutation for the same helium irradiation condition. It is clearly shown that the drift process leads to helium clusters trapped deeper in tungsten and the modified trap mutation process results in helium clusters segregated near the surface. The new Xolotl code was capable of predicating helium segregation on surfaces, consistent with MD simulation results [56] as shown in figure 8. Xolotl was later used to study the effects of grain boundaries [103], temperature and surface orientation [104]. Xolotl was further upgraded to implement the effect of bubble bursting [105]. The prediction of Xolotl matched better with the large-scale MD simulations recently reported by Hammond *et al* [57]

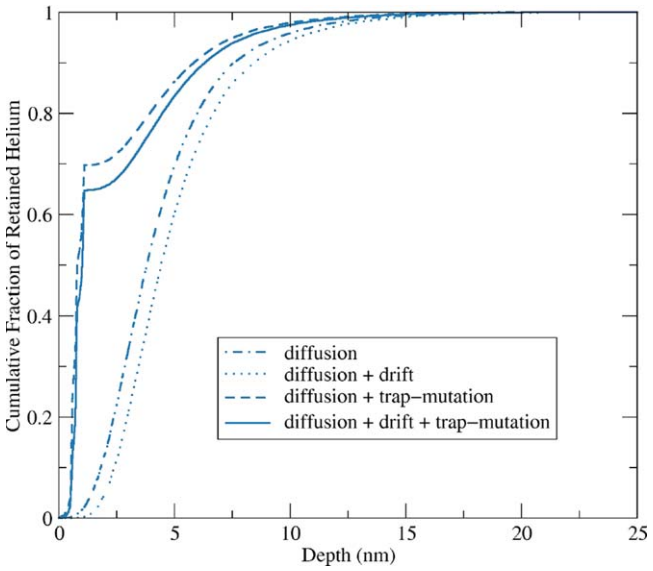

Figure 7. Comparison of cumulative helium distributions with and without considering the processes of drift and modified trap mutation. Reproduced from [78]. © IOP Publishing Ltd. All rights reserved.

after taking account of bubble bursting. However, the prediction was orders of magnitude away from the experimental results reported by Woller *et al* [106]. Blondel *et al* [105] then considered pre-existing defects or adjusted diffusion coefficients to achieve better agreement. However, they admitted that the reasoning for such an adjustment was not entirely clear.

In spite of this notable and encouraging progress, there are still many challenges that need to be addressed for a model with better predictive capability. For the modeling of long-term evolution of helium accumulations, we suggest the following research directions.

(1) It is important to explore new dominant mechanisms at an extended timescale beyond classical MD simulations by advanced simulation techniques, such as accelerated molecular dynamics (AMD) and atomistic kinetic Monte Carlo (AKMC) methods. As mentioned, the accuracy of predictions by OKMC and CD simulations depends on whether the essential physical processes are incorporated in the model and the accuracy of parameters (e.g. diffusion coefficients, binding energy, capture radius, etc). These physical processes and values of parameters are usually determined from DFT and MD simulations that can only deal with small temporal and spatial scales. As a result, some important processes beyond the capability of DFT and MD predictions may not be captured. For instance, small He–V complexes are usually considered as immobile. However, Perez *et al* [107] performed AMD simulations and discovered that such complexes can migrate on a timescale of milliseconds. By combination with CD simulations, they showed that the diffusion of small He–V complexes can provide an efficient pathway for helium release, leading to a significant decrease in helium concentration near

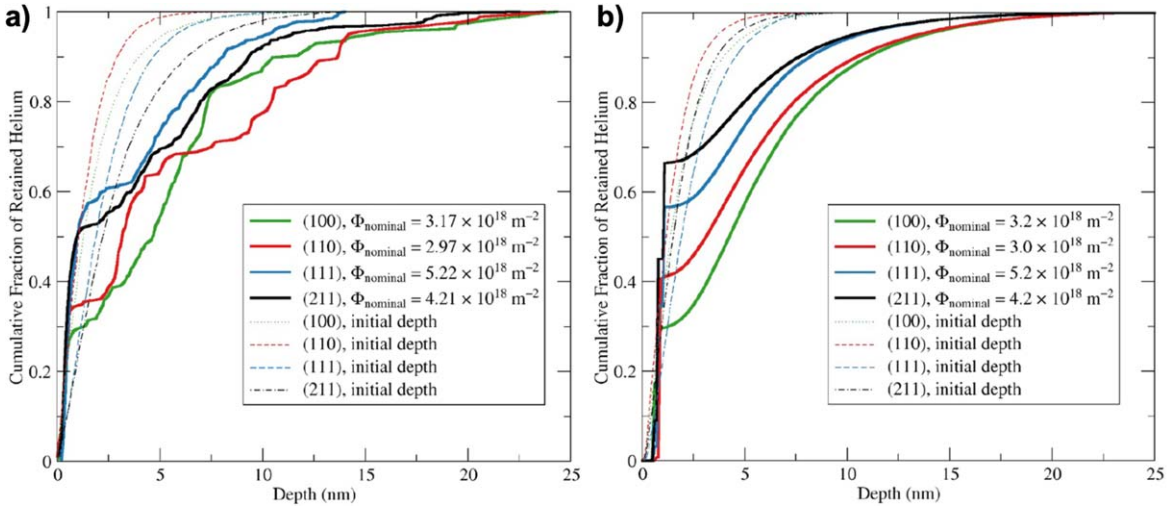

Figure 8. Cumulative helium distributions as a function of surface orientation at a helium flux of 4.0×10^{18} m^{-2} s^{-1} obtained by (a) MD simulations, (b) CD model. Reproduced from [78].

surface. Another example is the growth of helium bubbles at different growth rates. AMD simulations by Sandoval *et al* [108] revealed a biased growth of the bubble toward the surface at more realistic low rates, while classic MD simulations can only handle high growth rate and predicted a more isotropic growth, which leads to more surface damage. Moreover, currently the parameters for large-size clusters are interpolated from small-size clusters. Validation for such interpolation is also needed.

(2) It is necessary to identify the key processes and parameters used in the model and to quantify the uncertainty of the model to improve its reliability. This can be done by the application of uncertainty quantification (UQ) techniques [60, 109, 110] and sensitivity analysis (SA) [111–113].

(3) The influence of impurities has to be systematically evaluated. The currently used model assumes pure tungsten. In reality, impurities can come from material manufacturing, processing, plasma and neutron transmutation and strongly affect long-term evolution of helium bubble growth.

(4) The stress field around the over-pressurized bubbles and the loop-punching process needs to be taken into consideration. The stress field can change the reaction radii of helium atoms/clusters/bubbles with other defects. Dislocation loops punched out by bubbles can act as helium traps and nucleation sites for bubble formation, which could lead to the formation of a helium bubble network [81, 102].

(5) The model needs to be validated against more relevant experimental data.

3.2. Evolution of surface morphology and fuzz formation

The evolution of surface morphology at early stages has been greatly studied, mainly by MD simulations. It is generally accepted that the early-stage evolution is initiated by bubble growth and rupture. Sefta *et al* [114] revealed that adatom islands can be formed when dislocation loops punched out by an over-pressurized helium bubble annihilate at the surface, resulting in surface growth. In contrast, bubble rupture at the surface causes recession of the surface. Figure 9 shows a visualization of snapshots from the top view for large-scale, long-term MD simulations reported by Hammond *et al* [74, 115]. Surface islands and relatively large holes can be clearly seen from this image.

Several studies [116–119] employing either OKMC methods or hybrid approaches have attempted to extend MD predictions in order to investigate the evolution of surface morphology under interplay between different physical processes, including bubble growth, loop punching, bubble rupture, etc. Snapshots of surface morphology predicted from various studies are compiled in figure 10. Most of these studies predicted that the surface roughness was proportional to the square root of irradiation time, in good agreement with experimental observations. These studies confirm that the interplay between loop punching and bubble rupture can lead to the growth of surface structures and the increase of surface roughness. However, it is still arguable whether these structures can be called fuzz since the average diameter, spacing and shape are very different from experimental observations. For instance, most of the tendril-like structures in figure 10 have sizes of several nanometers, whereas the diameters of tendrils observed in experiments are usually several tens of nanometers. There are too many arbitrary simplifications and assumptions involved in these extended models, which influence the reliability of the predictions.

Recently, a continuum model was developed to investigate helium-induced surface evolution [120–124]. The model takes into account the self-interstitial flux from the bubble layer to the surface and the diffusion of surface adatoms, and subsurface bubble dynamics are ignored [120]. The simulated morphology and surface profile were qualitatively consistent with experimental observations. The model was later used to

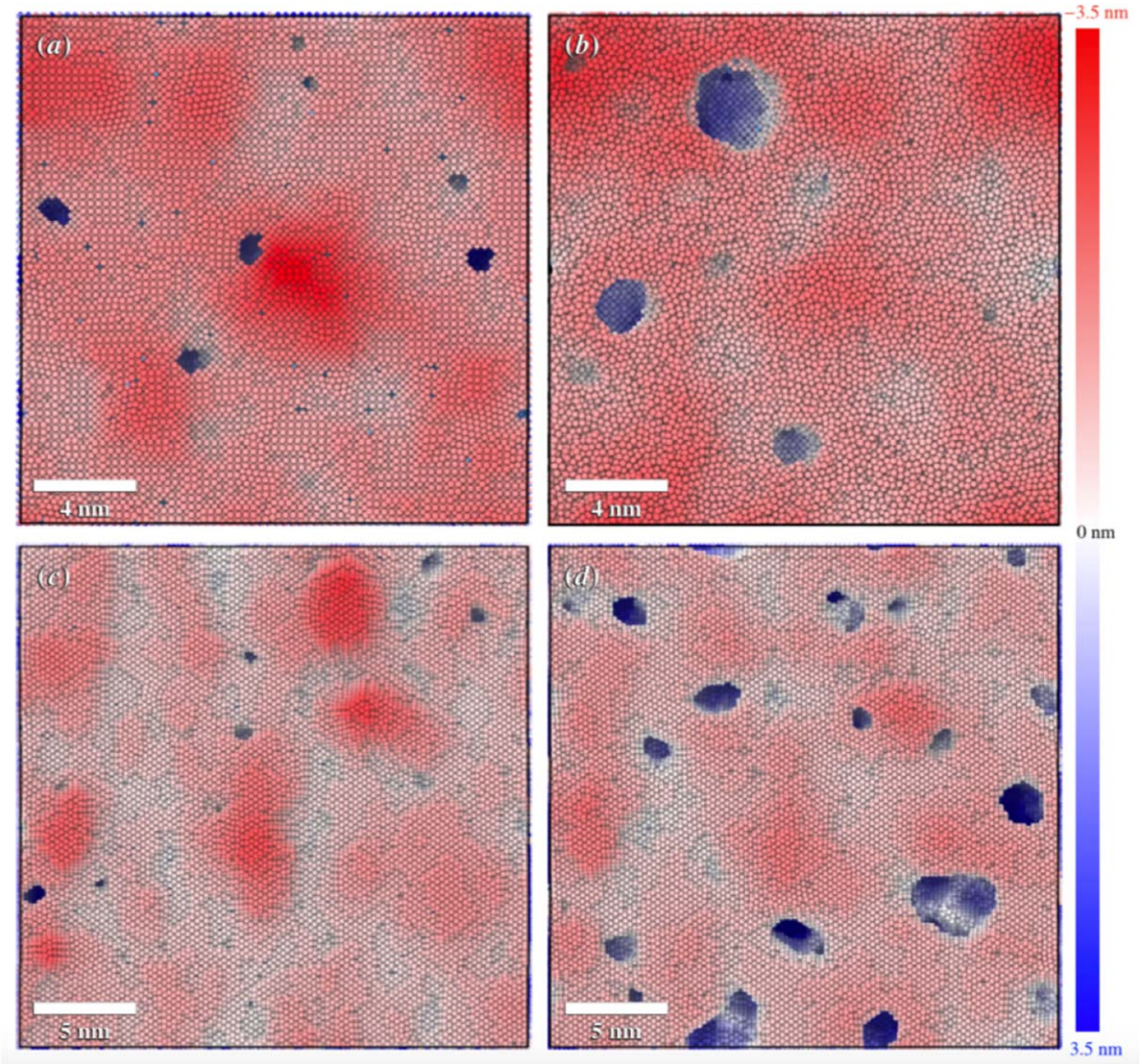

Figure 9. Visualization of snapshots from the top view for large-scale, long-term MD simulations. (a) and (b) are taken at the same location of a (001) surface at time of 77.900 ns and 77.9475 ns, respectively. (c) and (d) are taken at the same location of a (011) surface at time of 2.2400 μs and 2.2425 μs, respectively. The colors indicate the locations of atoms relative to the original surface. Reproduced from [74].

study the effects of temperature [121], elastic softening [122] and hole formation [123] on surface morphological evolution. Despite there still being a discrepancy between the model predictions and experimental observations, such continuum models have great potential to couple with CD simulations to reach temporal and spatial scales of fuzz formation in experiments.

In contrast to the early-stage growth, the mechanism for late-stage fuzz growth is still debatable. Recently, Wright [125] went through all proposed mechanisms in the literature and assessed them against experimental results. The supply of tungsten atoms to the fuzz layer was attributed to adatoms generated by loop punching, rather than viscoelastic effects [126] or adatoms generated directly by helium bombardment [127, 128]. Adatom formation requires helium bubble growth in the base of the fuzz layer. Cusentino *et al* [129] proposed the possibility of helium diffusion along fuzz tendrils to the base. However, their derivation of diffusivity in the tendrils was made upon assumptions of no absorption by traps. Another theory was proposed by Klaver *et al* [130, 131] and Yang *et al* [132]. Ellipsoids or cylinders (see figure 11) were used to construct fuzz layers. It was found that helium can reach hundreds of nanometers or even several micrometers deep into the fuzz just by ballistic collisions. Therefore, helium transport to the base of fuzz layers is likely through ballistic collisions. The contribution of helium diffusion needs further investigation.

3.3. Integrated model for plasma–material interactions under fusion operation conditions

So far, we have only discussed how plasma exposure changes surface properties of tungsten. However, the interactions are between both sides. The changes of tungsten surface can influence the local plasma conditions, which can in turn cause a

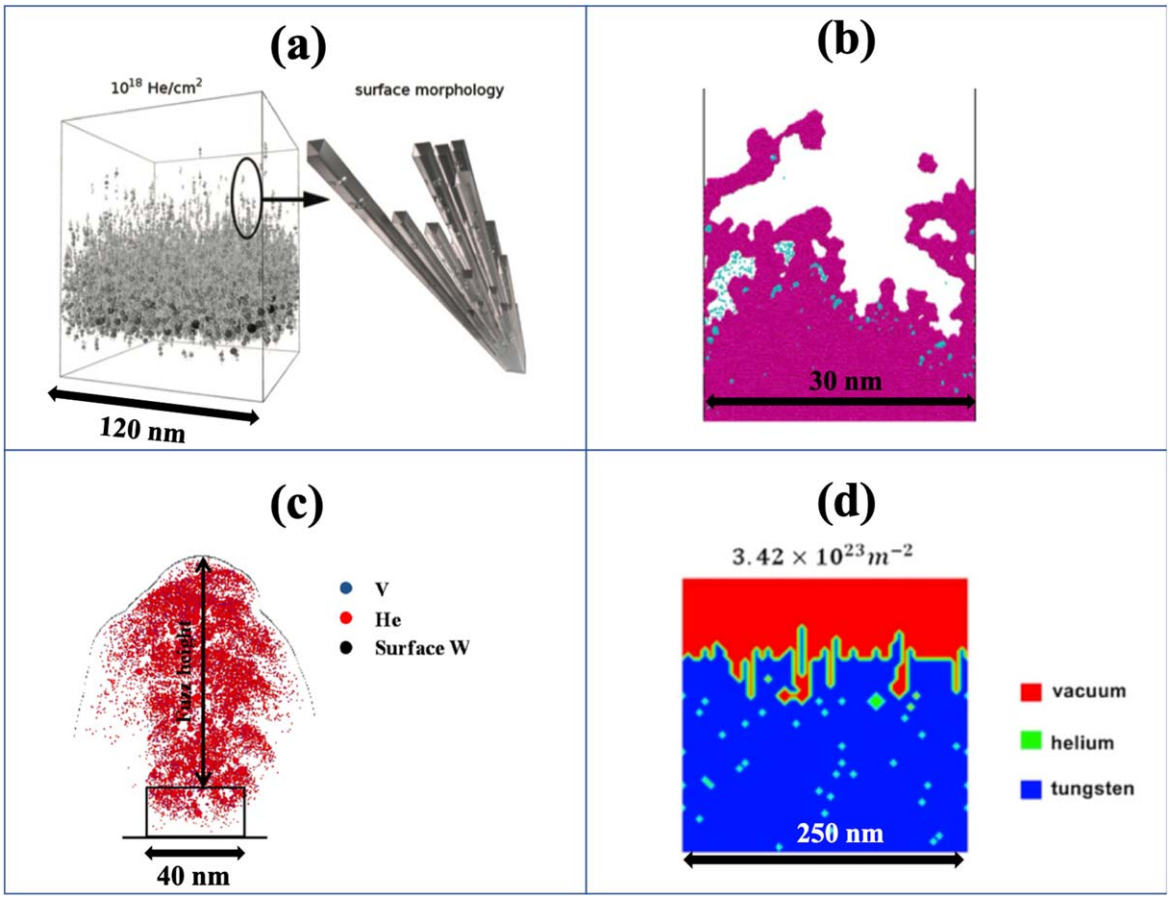

Figure 10. Snapshots of predicted surface morphology from various studies by (a) Lasa *et al*. Reproduced from [116]. © IOP Publishing Ltd All rights reserved; (b) Ito *et al.* Reproduced from [117]. © IOP Publishing Ltd. All rights reserved; (c) Valles *et al.* Reprinted from [118], Copyright (2017), with permission from Elsevier; (d) Shi *et al.* Reprinted from [119], Copyright (2018), with permission from Elsevier.

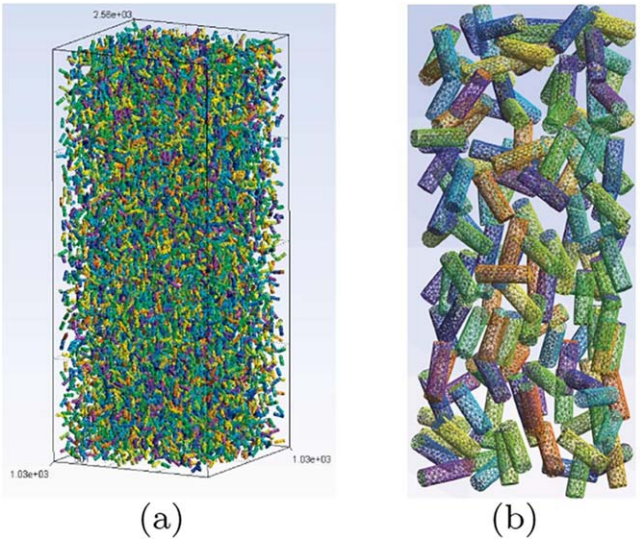

Figure 11. Side view of the fuzz generated by building blocks of cylinders. Figure (b) is the enlargement of a part in (a). Reprinted from [132], Copyright (2019), with permission from Elsevier.

feedback to the tungsten surface. For instance, a sputtered tungsten atom can go to the edge plasma, transport, and bombard back to the tungsten surface, causing redeposition and extra sputtering. The tungsten deposition flux is estimated to be around $10^{18}\,\mathrm{m}^{-2}\,\mathrm{s}^{-1}$ in ITER [133]. Recently, it was found that the growth of fuzz can be significantly enhanced by co-deposition of tungsten [134–137]. As shown in figure 12, fuzz growth under such co-deposition conditions can reach several millimeters and can be seen directly with the naked eye. Moreover, impurities (Ne, Ar, N_2) in helium plasma have also been found to cause the formation of nano-tendril bundles [138, 139]. Thus, the growth kinetic of structures on material surfaces can be dramatically altered by the feedback of plasma. The coupling between the surface of PFMs and the edge plasma physics is important for accurate predictions of dynamic PFMs under fusion operation conditions.

Recently, Lasa *et al* [140, 141] reported an integrated model coupling the background plasma transport, the near-surface sheath effects, the erosion and transport of wall materials across the scrape-off layer (SOF), sputtering and implantation of ions impacting on the material, and the dynamics of the subsurface gas atoms. The workflow of the model is shown in figure 13. The integrated model is still under development. More validations against experiments are required. Moreover, the current model only considers information passed from the plasma to the material side. The feedback of materials to the plasma needs to be included for future development.

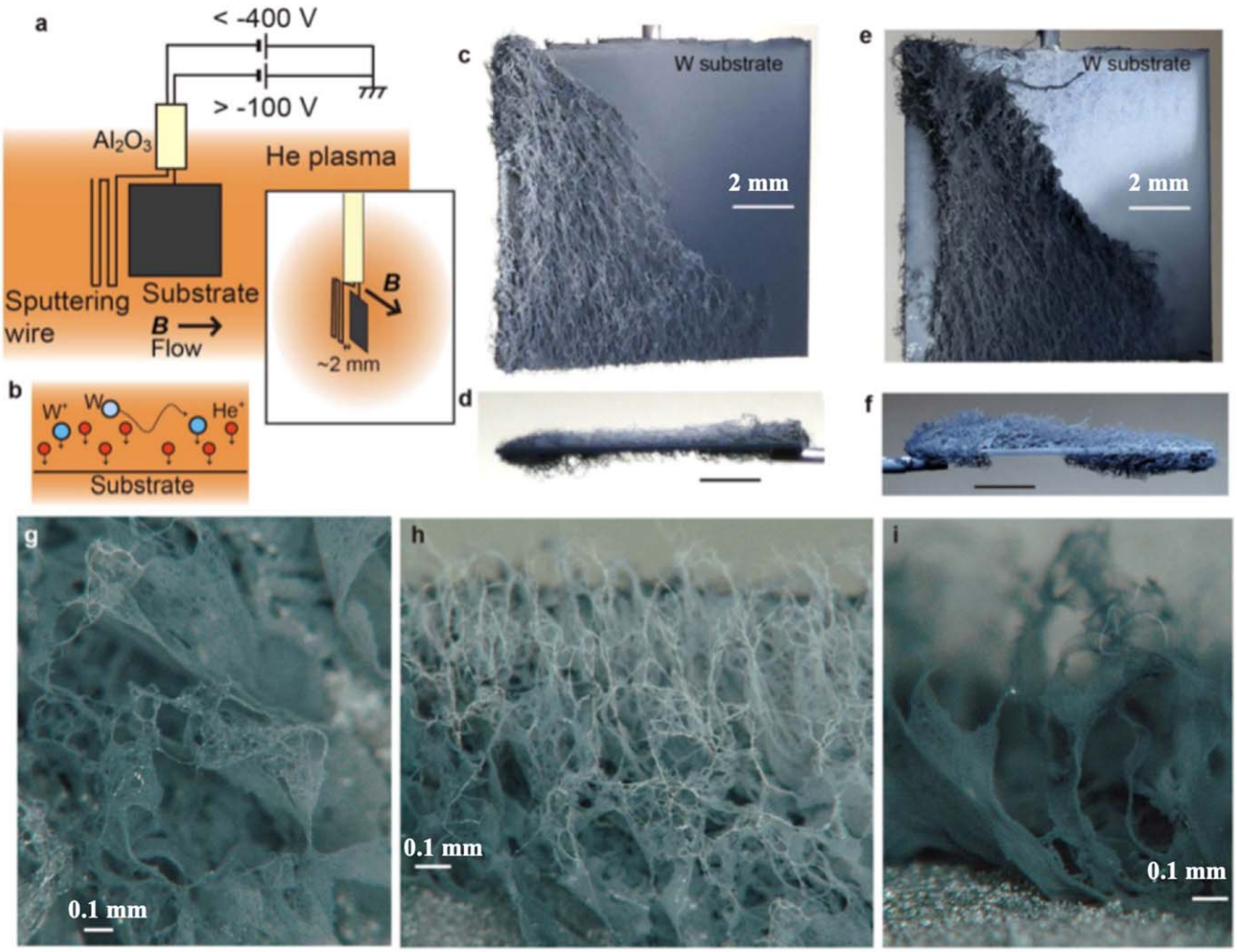

Figure 12. Micrographs of fuzz with co-deposition of tungsten. Reproduced from [134]. CC BY 4.0.

4. Change of properties of tungsten irradiated with helium

4.1. Sputtering

The sputtering property of a tungsten surface exposed to low-energy helium plasma can be changed by two factors, namely, bubbles underneath the surface and nanostructures on the surface. Currently, the former factor is seldom studied. MD simulations by Sefta *et al* [142] and Ferroni *et al* [143] indicated that the pre-existing helium bubbles have a negligible effect on the tungsten sputtering yield for helium ions with energy of 200–500 eV. Further investigations are needed to gain more knowledge for different ion species with a broad range of energies.

In contrast, the influence of surface nanostructures on sputtering has been investigated in great detail. Li *et al* [144] used a BCA-based approach to study the influence of surface roughness on sputtering yield. They found that the increase in surface roughness decreases the sputtering yield. This effect was mainly attributed to the re-deposition of sputtered atoms to neighboring structures. Several models [132, 145–147] as shown in figure 14 have been proposed to study the sputtering yield of fuzz structures by constructing a 3D structure of fuzz. The influence of some important factors, including ion energies, incidence angles and fuzz thickness, were studied. These models also attributed the reduction in the sputtering yield of a fuzz layer to the effect of re-deposition of sputtered atoms. However, the geometric shape of the tendrils in these models are different from experimental observations, which could potentially cause uncertainties in the validity of the models since it is known that sputtering yields depend strongly on impact angles [148] and surface curvatures [149, 150]. Moreover, an analytical relation would be more desirable for coupling with other continuum approaches. Recently, Fan *et al* [37] developed an analytical model for calculations of sputtering yield of fuzz layers. The analytical model relies on an important parameter, namely, the mean free path of incident ions, which was assumed to be dependent on the radius of nano-tendrils and the density of the fuzz layer. This is a first-order approximation, ignoring the alignment and the intersection of the tendrils. We suggest combining the 3D structure modeling with the analytical model to achieve a better model with fully predictive capability since the mean free path of an energetic particle in a fuzz layer can be obtained in a more accurate way by the model using the 3D structure of fuzz [132].

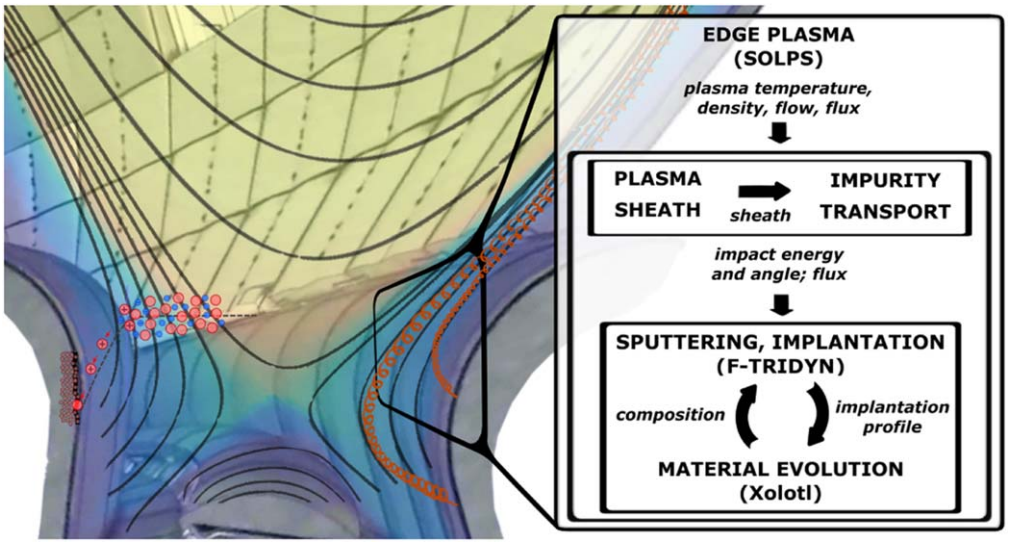

Figure 13. Workflow of the integrated model developed by Lasa *et al.* Reproduced from [140]. © IOP Publishing Ltd. All rights reserved.

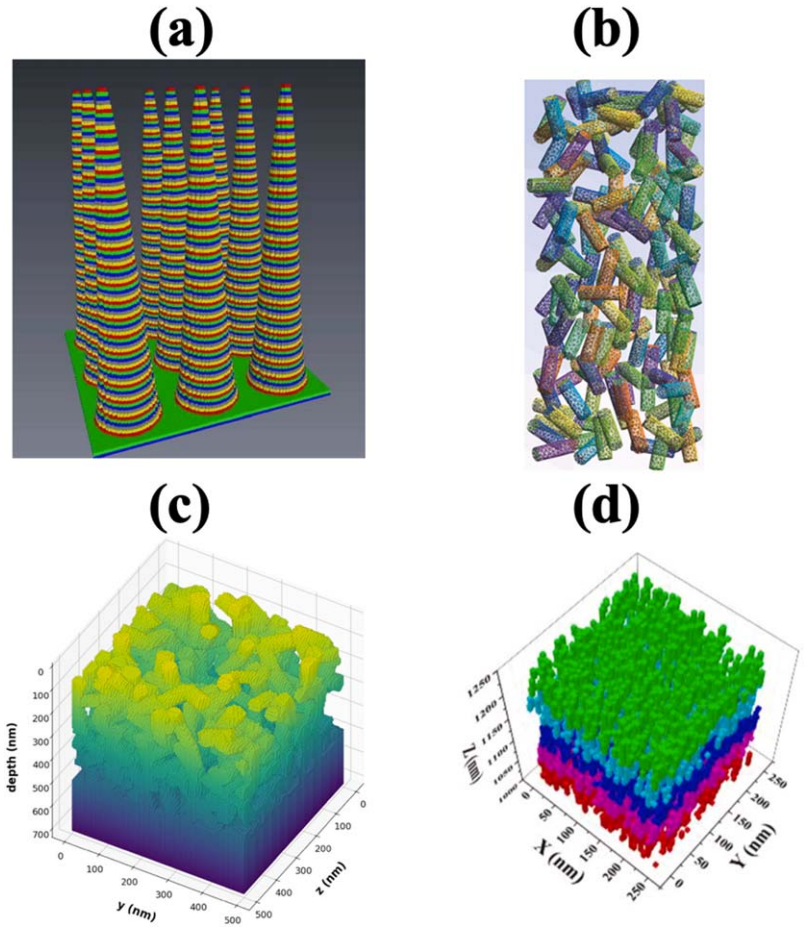

Figure 14. Fuzz structures developed by different studies. (a) Reproduced from [145]. © IOP Publishing Ltd. All rights reserved. (b) Reprinted from [132], Copyright (2019), with permission from Elsevier. (c) Reprinted from [146], Copyright (2020), with permission from Elsevier. (d) Reprinted from [147], Copyright (2022), with permission from Elsevier.

4.2. Thermal properties

In solids, heat is conducted mainly by two mechanisms, namely, electron thermal conduction and phonon/lattice thermal conduction. In metals, the former is the dominant mechanism. However, first-principles calculations by Chen *et al* [151] revealed that the contribution from phonons is about one third of that from electrons for pure tungsten at

room temperature, which means that phonon thermal conduction cannot be ignored for tungsten. The degradation of thermal conductivity caused by low-energy helium exposure is only limited to local regions, at most a few micrometers beneath the surface. Although a significant portion of helium may diffuse deep into tungsten beyond the subsurface region, these helium atoms will be trapped by the grain boundaries which are strong traps for helium [70, 76]. As a result, the trapping depth of the implanted helium is limited by the grain size of tungsten which is a few micrometers for ITER-grade tungsten.

The degradation of thermal conductivity for helium-implanted surfaces is caused by two factors, namely, the extreme low thermal conductivity of helium which is several orders of magnitude lower than tungsten [152], and the increase in electron scattering and phonon scattering caused by helium-related defects. By taking account of only the former reason, Wang *et al* [152] estimated a decrease of about 30% in thermal conductivity for a 30% volume fraction of helium bubbles using finite element methods. Using MD methods, Hu *et al* [153] found that helium bubbles induce a larger decrease in thermal conductivity than voids of the same size due to phonon scattering by helium bubbles. Ding *et al* [154] indicated that thermal resistance increases when there are helium bubbles at grain boundaries.

In addition to reduction of the thermal conductivity by the presence of a high density of helium bubbles and grain boundaries in nano-tendrils, the thermal conductivity of fuzz can be further reduced by the small size of nano-tendrils. Hu *et al* [155] studied thermal transport in tungsten nanowires using first-principles calculations and found that both the electronic and phonon thermal conductivities are reduced compared to the bulk and smaller size of nanowires lead to more reductions. To our knowledge, no models or theories have been established to model the thermal conductivity of fuzz layers. We suggest that a combination of atomistic simulations and theories for porous materials [156, 157] could be a potential approach for the establishment of such a model.

5. Summary

We have overviewed the recent progress, gaps and challenges in the modeling and simulations of long-term response of tungsten under exposure of low-energy helium plasma. Following the trajectory of impinging helium ions, we first overviewed the implantation and clustering processes of helium atoms. Numerous DFT and MD studies have been carried out and the mechanisms of helium bubble nucleation and growth have been revealed. Due to the low energies, no displacement damages are generated by collisions of impinging ions with tungsten atoms, and many-body atomic interactions may play an important role in calculations of reflection coefficients and implantation depth distributions. The high mobility of the implanted helium atoms and the strong attraction between helium atoms and other defects, such as vacancies and helium atoms, lead to the trapping of helium atoms and nucleation of helium bubbles. A database of the thermodynamic and kinetic properties of helium atoms/clusters/bubbles and defect complexes can be established based on these atomic simulations, serving as input parameters for higher-level simulations. We noted that particular attention needs to be paid to the dynamics of small helium clusters near surfaces.

The enormous efforts put into atomistic simulations have built a solid foundation for a higher level of simulations accounting for the long-term evolution of helium accumulation and surface morphology. As a result, notable progress has been made in the modeling of long-term evolution of subsurface helium bubbles. In particular, by taking into account the surface effects, the CD code Xolotl is capable of predicting the evolution of helium bubbles which is in good agreement with the large-scale MD simulations. Certainly, additional efforts are required to reach better agreement with experimental results.

The evolution of the surface morphology at early stages has been attributed to the interplay between different physical processes including bubble growth, loop punching, bubble rupture and adatom diffusion. Since the mechanism for late-stage growth of surface structures is still under debate, we discussed various theories proposed in the literature and provided suggestions for possible mechanisms. The modeling and simulations of sputtering and thermal properties, and the integration of different modeling codes into a framework, are at the initial stage of development but some promising results have been obtained.

In spite of these notable and encouraging progresses, establishing a predictive modeling capability for dynamic evolution of PFM under fusion operation conditions is still very challenging and more efforts are definitely required. We suggest the following research directions for future investigations: (i) using AMD methods to study new mechanisms that may dominate at timescales beyond the capability of classical MD methods; (ii) a better coupling scheme to integrate subsurface helium accumulation, evolution of surface morphology and changes in properties; and (iii) synergetic effects of helium/hydrogen plasma exposure and neutron irradiation.

Acknowledgments

This work was supported by National Natural Science Foundation of China (No. 11905071) and the National MCF Energy R&D Program (No. 2018YFE0308103).

ORCID iDs

Zhangcan YANG (杨章灿) https://orcid.org/0000-0002-5621-6789

References

[1] Ye M Y 2005 *Plasma Sci. Technol.* **7** 2828
[2] Pintsuk G 2012 Tungsten as a plasma-facing material ed R J M Konings *Comprehensive Nuclear Materials* (Amsterdam: Elsevier) 551

[3] Ueda Y *et al* 2014 *Fusion Eng. Des.* **89** 901
[4] Hammond K D 2017 *Mater. Res. Express* **4** 104002
[5] Marian J *et al* 2017 *Nucl. Fusion* **57** 092008
[6] Rieth M *et al* 2019 *J. Nucl. Mater.* **519** 334
[7] De Temmerman G, Hirai T and Pitts R A 2018 *Plasma Phys. Control. Fusion* **60** 044018
[8] Li Y G *et al* 2020 *Tungsten* **2** 34
[9] Meyer F W *et al* 2014 *J. Phys. Conf. Ser.* **488** 012036
[10] Meyer F W *et al* 2014 *Phys. Scr.* **2014** 014029
[11] Wang K *et al* 2017 *Sci. Rep.* **7** 42315
[12] Bernard E *et al* 2015 *J. Nucl. Mater.* **463** 316
[13] Miyamoto M *et al* 2015 *J. Nucl. Mater.* **463** 333
[14] Liu F S *et al* 2014 *Fusion Eng. Des.* **89** 2516
[15] Garrison L M and Kulcinski G L 2015 *J. Nucl. Mater.* **466** 302
[16] Thompson M *et al* 2018 *Nucl. Fusion* **58** 066010
[17] Wang S W *et al* 2020 *J. Nucl. Mater.* **532** 152051
[18] Wu X B *et al* 2014 *J. Nucl. Mater.* **455** 151
[19] Zhao Q *et al* 2019 *Comput. Mater. Sci.* **162** 133
[20] Yue F Y *et al* 2021 *J. Nucl. Mater.* **543** 152545
[21] Parish C M *et al* 2014 *Acta Mater.* **62** 173
[22] El-Atwani O *et al* 2012 *J. Nucl. Mater.* **434** 170
[23] El-Atwani O *et al* 2014 *Nucl. Fusion* **54** 083013
[24] Chen Z *et al* 2018 *Acta Mater.* **147** 100
[25] El-Atwani O *et al* 2020 *J. Nucl. Mater.* **538** 152150
[26] Baldwin M J *et al* 2009 *J. Nucl. Mater.* **390–391** 886
[27] Baldwin M J *et al* 2011 *Nucl. Fusion* **51** 103021
[28] De Temmerman G *et al* 2013 *J. Nucl. Mater.* **438** S78
[29] Baldwin M J and Doerner R P 2008 *Nucl. Fusion* **48** 035001
[30] Takamura S *et al* 2006 *Plasma Fusion Res.* **1** 051
[31] Wright G M *et al* 2012 *Nucl. Fusion* **52** 042003
[32] Fan H Y *et al* 2015 *Plasma Sci. Technol.* **17** 331
[33] Kajita S *et al* 2009 *Nucl. Fusion* **49** 095005
[34] Baldwin M J and Doerner R P 2010 *J. Nucl. Mater.* **404** 165
[35] Petty T J *et al* 2015 *Nucl. Fusion* **55** 093033
[36] Nishijima D *et al* 2004 *J. Nucl. Mater.* **329–333** 1029
[37] Fan H Y *et al* 2021 *Plasma Sci. Technol.* **24** 015601
[38] Miyamoto M *et al* 2011 *J. Nucl. Mater.* **415** S657
[39] Qu S L *et al* 2018 *Fusion Eng. Des.* **137** 97
[40] Kajita S *et al* 2016 *Results Phys.* **6** 877
[41] Kajita S *et al* 2016 *Jpn. J. Appl. Phys.* **55** 056203
[42] Qu S L *et al* 2017 *J. Nucl. Mater.* **484** 382
[43] Kajita S, Takamura S and Ohno N 2009 *Nucl. Fusion* **49** 032002
[44] Nishijima D *et al* 2013 *J. Nucl. Mater.* **434** 230
[45] Kajita S 2014 *Nucl. Fusion* **54** 033005
[46] Sinclair G, Tripathi J K and Hassanein A 2018 *J. Appl. Phys.* **123** 133302
[47] Takanori M, Shuichi T and Hiroaki K 2013 *Plasma Sci. Technol.* **15** 161
[48] Tokitani M *et al* 2011 *Nucl. Fusion* **51** 102001
[49] Rudakov D L *et al* 2016 *Phys. Scr.* **2016** 014055
[50] Nishijima D *et al* 2011 *J. Nucl. Mater.* **415** S96
[51] Wirth B D *et al* 2015 *J. Nucl. Mater.* **463** 30
[52] Sandoval L *et al* 2019 *Materials* **12** 2500
[53] Ziegler J F, Ziegler M D and Biersack J P 2010 *Nucl. Instrum. Methods Phys. Res. Sect. B: Beam Interact. Mater. Atoms* **268** 1818
[54] Henriksson K O E, Nordlund K and Keinonen J 2006 *Nucl. Instrum. Methods Phys. Res. Sect. B: Beam Interact. Mater. Atoms* **244** 377
[55] Pentecoste L *et al* 2016 *J. Nucl. Mater.* **470** 44
[56] Hammond K D and Wirth B D 2014 *J. Appl. Phys.* **116** 143301
[57] Hammond K D *et al* 2018 *Acta Mater.* **144** 561
[58] Yang Z C *et al* 2017 *Fusion Sci. Technol.* **71** 60
[59] Faney T and Wirth B D 2014 *Modelling Simul. Mater. Sci. Eng.* **22** 065010
[60] Cekmer O *et al* 2018 *Int. J. Uncertainty Quantif.* **8** 429
[61] Cusentino M A, Wood M A and Thompson A P 2020 *Nucl. Fusion* **60** 126018
[62] Becquart C S and Domain C 2006 *Phys. Rev. Lett.* **97** 196402
[63] Wang J *et al* 2012 *J. Nucl. Mater.* **427** 290
[64] Perez D, Vogel T and Uberuaga B P 2014 *Phys. Rev.* B **90** 014102
[65] Shu X L *et al* 2013 *Nucl. Instrum. Methods Phys. Res. Sect. B: Beam Interact. Mater. Atoms* **303** 84
[66] Boisse J, Domain C and Becquart C S 2014 *J. Nucl. Mater.* **455** 10
[67] Li X C 2014 *J. Nucl. Mater.* **451** 356
[68] Becquart C S and Domain C 2009 *J. Nucl. Mater.* **385** 223
[69] Wu X B *et al* 2013 *Nucl. Fusion* **53** 073049
[70] Hammond K D *et al* 2015 *Europhys. Lett.* **110** 52002
[71] Wang J L *et al* 2015 *Nucl. Fusion* **55** 092003
[72] Yang Z C and Hammond K D 2018 *J. Phys. Condens. Matter* **30** 325002
[73] Kobayashi R *et al* 2015 *J. Nucl. Mater.* **463** 1071
[74] Hammond K D *et al* 2019 *Nucl. Fusion* **59** 066035
[75] Hu L *et al* 2014 *Surf. Sci.* **626** L21
[76] Hu L *et al* 2014 *J. Appl. Phys.* **115** 173512
[77] Hu L *et al* 2015 *J. Appl. Phys.* **118** 163301
[78] Maroudas D *et al* 2016 *J. Phys. Condens. Matter* **28** 064004
[79] Perez D *et al* 2016 *J. Appl. Phys.* **119** 203301
[80] Wang X X, Niu L L and Wang S Q 2017 *J. Nucl. Mater.* **487** 158
[81] Sandoval L *et al* 2018 *Acta Mater.* **159** 46
[82] Xie H X *et al* 2017 *Acta Mater.* **141** 10
[83] Smirnov R D, Krasheninnikov S I and Guterl J 2015 *J. Nucl. Mater.* **463** 359
[84] Zhan J *et al* 2021 *Comput. Mater. Sci.* **187** 110076
[85] Xu Y and Yang Z C 2022 *At. Energy Sci. Technol.* **56** 168 (in Chinese)
[86] Faney T, Krasheninnikov S I and Wirth B D 2015 *Nucl. Fusion* **55** 013014
[87] Domain C and Becquart C S 2018 Object Kinetic Monte Carlo (OKMC): a coarse-grained approach to radiation damage *Handbook of Materials Modeling: Methods: Theory and Modeling* ed W Andreoni and S Yip (Berlin: Springer) 1287
[88] Becquart C S *et al* 2010 *J. Nucl. Mater.* **403** 75
[89] Nandipati G *et al* 2022 *J. Phys. Condens. Matter* **34** 035701
[90] Ma F F *et al* 2021 *Nucl. Fusion* **61** 106017
[91] Hou P W *et al* 2021 *Chin. Phys.* B **30** 086108
[92] Hou J *et al* 2016 *Comput. Mater. Sci.* **123** 148
[93] Golubov S I, Barashev A V and Stoller R E 2020 Reaction rate theory ed R J M Konings and R E Stoller *Comprehensive Nuclear Materials* 2nd edn (Amsterdam: Elsevier) 717
[94] Kohnert A A, Wirth B D and Capolungo L 2018 *Comput. Mater. Sci.* **149** 442
[95] Watanabe Y *et al* 2007 *Nucl. Instrum. Methods Phys. Res. Sect. B: Beam Interact. Mater. Atoms* **255** 32
[96] Xu Q, Yoshida N and Yoshiie T 2007 *J. Nucl. Mater.* **367–370** 806
[97] Li Y G *et al* 2012 *Commun. Comput. Phys.* **11** 1547
[98] Li Y G *et al* 2012 *J. Nucl. Mater.* **431** 26
[99] Zhao Z *et al* 2017 *Nucl. Fusion* **57** 086020
[100] Krasheninnikov S I, Faney T and Wirth B D 2014 *Nucl. Fusion* **54** 073019
[101] Krasheninnikov S I and Smirnov R D 2015 *Nucl. Fusion* **55** 073005
[102] Krasheninnikov S I and Smirnov R D 2016 *Phys. Scr.* **2016** 014021
[103] Blondel S *et al* 2017 *Fusion Sci. Technol.* **71** 84
[104] Blondel S *et al* 2017 *Fusion Sci. Technol.* **71** 22
[105] Blondel S *et al* 2018 *Nucl. Fusion* **58** 126034
[106] Woller K B, Whyte D G and Wright G M 2015 *J. Nucl. Mater.* **463** 289

[107] Perez D *et al* 2017 *Sci. Rep.* **7** 2522
[108] Sandoval L *et al* 2015 *Phys. Rev. Lett.* **114** 105502
[109] Chernatynskiy A, Phillpot S R and LeSar R 2013 *Annu. Rev. Mater. Res.* **43** 157
[110] Wang Y and McDowell D L 2020 Uncertainty quantification in materials modeling ed Y Wang and D L McDowell *Uncertainty Quantification in Multiscale Materials Modeling* (Cambridge, MA: Woodhead Publishing) 1
[111] Saltelli A *et al* 2007 *Global Sensitivity Analysis. The Primer* (Chichester: Wiley)
[112] Looss B and Lemaître P 2015 A review on global sensitivity analysis methods ed G Dellino and C Meloni *Uncertainty Management in Simulation-Optimization of Complex Systems: Algorithms and Applications* (Boston, MA: Springer) 101
[113] Ye M and Hill M C 2017 Global sensitivity analysis for uncertain parameters, models, and scenarios ed G P Petropoulos and P K Srivastava *Sensitivity Analysis in Earth Observation Modelling* (Amsterdam: Elsevier) 177
[114] Sefta F *et al* 2013 *Nucl. Fusion* **53** 073015
[115] Hammond K D *et al* 2020 *Nucl. Fusion* **60** 129401
[116] Lasa A, Tähtinen S K and Nordlund K 2014 *Europhys. Lett.* **105** 25002
[117] Ito A M *et al* 2015 *Nucl. Fusion* **55** 073013
[118] Valles G *et al* 2017 *J. Nucl. Mater.* **490** 108
[119] Shi Q, Dai S Y and Wang D Z 2018 *Fusion Eng. Des.* **136** 554
[120] Dasgupta D *et al* 2019 *Nucl. Fusion* **59** 086057
[121] Dasgupta D, Maroudas D and Wirth B D 2020 *Surf. Sci.* **698** 121614
[122] Chen C S *et al* 2021 *Nucl. Fusion* **61** 016016
[123] Chen C S *et al* 2021 *J. Appl. Phys.* **129** 193302
[124] Chen C S *et al* 2021 *Phys. Rev. Mater.* **5** 113403
[125] Wright J A R 2022 *Tungsten* **4** 184
[126] Krasheninnikov S I 2011 *Phys. Scr.* **2011** 014040
[127] Trufanov D, Marenkov E and Krasheninnikov S 2015 *Phys. Procedia* **71** 20
[128] Martynenko Y V and Nagel M Y 2012 *Plasma Phys. Rep.* **38** 996
[129] Cusentino M A and Wirth B D 2020 *Comput. Mater. Sci.* **183** 109875
[130] Klaver T P C *et al* 2016 *Nucl. Fusion* **56** 126015
[131] Klaver T P C, Zhang S and Nordlund K 2017 *J. Nucl. Mater.* **492** 113
[132] Yang Z C *et al* 2019 *Nucl. Instrum. Methods Phys. Res. Sect. B: Beam Interact. Mater. Atoms* **455** 118
[133] Schmid K *et al* 2015 *Nucl. Fusion* **55** 053015
[134] Kajita S *et al* 2018 *Sci. Rep.* **8** 56
[135] Kajita S *et al* 2018 *Nucl. Fusion* **58** 106002
[136] Kajita S, Yoshida N and Ohno N 2020 *Nucl. Mater. Energy* **25** 100828
[137] McCarthy P *et al* 2020 *Nucl. Fusion* **60** 026012
[138] Woller K B, Whyte D G and Wright G M 2017 *Nucl. Mater. Energy* **12** 1282
[139] Hwangbo D *et al* 2018 *Nucl. Fusion* **58** 096022
[140] Lasa A *et al* 2020 *Phys. Scr.* **2020** 014041
[141] Lasa A *et al* 2021 *Nucl. Fusion* **61** 116051
[142] Sefta F *et al* 2013 *J. Nucl. Mater.* **438** S493
[143] Ferroni F, Hammond K D and Wirth B D 2015 *J. Nucl. Mater.* **458** 419
[144] Li Y G *et al* 2017 *Nucl. Fusion* **57** 016038
[145] von Toussaint U, Mutzke A and Manhard A 2017 *Phys. Scr.* **2017** 014056
[146] Stadlmayr R *et al* 2020 *J. Nucl. Mater.* **532** 152019
[147] Liu D H *et al* 2022 *Nucl. Mater. Energy* **31** 101205
[148] Hofsäss H, Zhang K and Mutzke A 2014 *Appl. Surf. Sci.* **310** 134
[149] Nietiadi M L and Urbassek H M 2013 *Appl. Phys. Lett.* **103** 113108
[150] Bradley R M and Hofsäss H 2014 *J. Appl. Phys.* **116** 234304
[151] Chen Y N, Ma J L and Li W 2019 *Phys. Rev.* B **99** 020305(R)
[152] Wang Y Y and Zhao J J 2022 *Int. J. Heat Mass Transfer* **193** 122965
[153] Hu L, Wirth B D and Maroudas D 2017 *Appl. Phys. Lett.* **111** 081902
[154] Ding Y M *et al* 2021 *Fusion Eng. Des.* **168** 112682
[155] Hu Y, Li S H and Bao H 2021 *Phys. Rev.* B **103** 104301
[156] Loeb A L 1954 *J. Am. Ceram. Soc.* **37** 96
[157] Smith D S *et al* 2013 *J. Mater. Res.* **28** 2260